EMBRY-RIDDLE
Aeronautical University™
SCHOLARLY COMMONS

Publications

6-2013

70 DA White Dwarfs Identified in Lamost Pilot Survey

J. K. Zhao
Chinese Academy of Sciences, Beijing

A. L. Luo
Chinese Academy of Sciences, Beijing

Terry D. Oswalt
Florida Institute of Technology, oswalb32@erau.edu

G. Zhao
Florida Institute of Technology - Melbourne

Follow this and additional works at: https://commons.erau.edu/publication

Part of the Stars, Interstellar Medium and the Galaxy Commons

Scholarly Commons Citation

70 DA WHITE DWARFS IDENTIFIED IN LAMOST PILOT SURVEY

J. K. ZHAO[1], A. L. LUO[1], T. D. OSWALT[2], AND G. ZHAO[1]
[1] Key Laboratory of Optical Astronomy, National Astronomical Observatories, Chinese Academy of Sciences,
Beijing 100012, China; zjk@bao.ac.cn, gzhao@bao.ac.cn, lal@bao.ac.cn
[2] Physics and Space Science Department, Florida Institute of Technology, Melbourne, FL 32901, USA; toswalt@fit.edu

ABSTRACT

We present a spectroscopically identified catalog of 70 DA white dwarfs (WDs) from the LAMOST pilot survey. Thirty-five are found to be new identifications after cross-correlation with the Eisenstein et al. and Villanova catalogs. The effective temperature and gravity of these WDs are estimated by Balmer lines fitting. Most of them are hot WDs. The cooling times and masses of these WDs are estimated by interpolation in theoretical evolution tracks. The peak of the mass distribution is found to be ∼0.6 $M_\odot$, which is consistent with prior work in the literature. The distances of these WDs are estimated using the method of synthetic spectral distances. All of these WDs are found to be in the Galactic disk from our analysis of space motions. Our sample supports the expectation that WDs with high mass are concentrated near the plane of the Galactic disk.

Key word: white dwarfs

Online-only material: color figure

1. INTRODUCTION

White dwarfs (WDs) are the final stage for the evolution of the majority of low- and medium-mass stars with initial masses < 8 $M_\odot$. Since there are no fusion reaction, the evolution of WDs is primarily determined by a well-understood cooling process (Fontaine et al. 2001; Salaris et al. 2000). Thus, they can be used for cosmochronology, an independent age-dating method. Also, the luminosity function of WDs provides firm constraints on the local star formation rate and history of the Galactic disk (Krzesinski et al. 2009).

McCook & Sion (1999) present a catalog of 2249 WDs that have been identified spectroscopically. In addition, the Sloan Digital Sky Survey (SDSS; York et al. 2000) has greatly expanded the number of spectroscopically confirmed WD stars (Harris et al. 2003; Kleinman et al. 2004, 2013; Eisenstein et al. 2006). The latter presented a catalog of 20,407 spectroscopically confirmed WDs from the SDSS Data Release 4 (DR4), roughly doubling the number of spectroscopically confirmed WDs.

Large sky Area Multi-Object Fiber Spectroscopic Telescope (LAMOST, so-called the Guoshoujing Telescope) is a National Major Scientific Project undertaken by the Chinese Academy of Science (Wang et al. 1996; Cui et al. 2012). LAMOST has recently completed the pilot survey from 2011 October to 2012 May, which obtained several hundred thousand spectra (Luo et al. 2012). From 2012 September, LAMOST has undertaken the general survey and will observe about 1 million stars per year. LAMOST has the capability to observe large, deep, and dense regions in the Milky Way Galaxy, which will enable a number of research topics to explore the evolution and the structure of the Milky Way. Therefore, it will definitely yield a large sample of WDs.

WDs whose primary spectral classification is DA have hydrogen-dominated atmospheres. They make up the majority (approximately 75%) of all observed WDs (Fontaine & Wesemael 2000). Such WDs are easy to identify using optical spectra. Here, we present a catalog of DA WDs from the LAMOST pilot survey (Luo et al. 2012). We do not expect the completeness of this sample. In Section 2, we describe the

spectra obtained. Section 3 discusses how the T_{eff}, log g, mass, and distance of the WDs were estimated. The kinematics of these WDs are illustrated in Section 4. A summary of our pilot study results is given in Section 5.

2. LAMOST PILOT DATA AND OBSERVATIONS

The LAMOST spectra have a resolving power of $R \sim 2000$ spanning 3700–9000 Å. Two arms of each spectrograph cover this wavelength range with overlap of 200 Å. The blue spectral coverage is 3700–5900 Å, while that in the red is 5700–9000 Å. The raw data were reduced with LAMOST two-dimensional and one-dimensional pipelines (Luo et al. 2004). These pipelines include bias subtraction, cosmic-ray removal, spectral trace and extraction, flat fielding, wavelength calibration, sky subtraction, and combination. The throughput in the red band is higher than the blue band.

The pilot survey obtained spectra of stars in the Milky Way, which included fainter objects on dark nights (Yang et al. 2012; Carlin et al. 2012), brighter objects on bright nights (Zhang et al. 2012), objects in the disk of the Galaxy with low latitude (Chen et al. 2012), and objects in the region of the Galactic anticenter. It also targets extragalactic objects located in two regions, i.e., the south Galactic cap and the north Galactic cap.

We found 20 WD spectra in both SDSS and LAMOST pilot survey catalogs. Figure 1 shows a portion of a typical spectrum. The top panel compares the SDSS DR7 and LAMOST spectra for the object J100316.35−002336.95. The solid line is the SDSS spectrum. The dotted line is the LAMOST spectrum. The bottom panel shows the residual between two spectra. The mean difference between two spectra is less than 10%.

The initial WD candidates we selected are from two sources. One is the LAMOST pipeline (Luo et al. 2012), which yielded about 2000 candidates using the "PCAZ" method. For stars with SDSS photometry, we used formulae (1)–(4) of Eisenstein et al. (2006) to identify candidates. Next, each of these spectra was inspected by eye. Stars with signal-to-noise ratio (S/N) smaller than 10 were excluded. Finally, if the Balmer line profiles of the star were a little too narrow (log g < 7.0), the spectrum
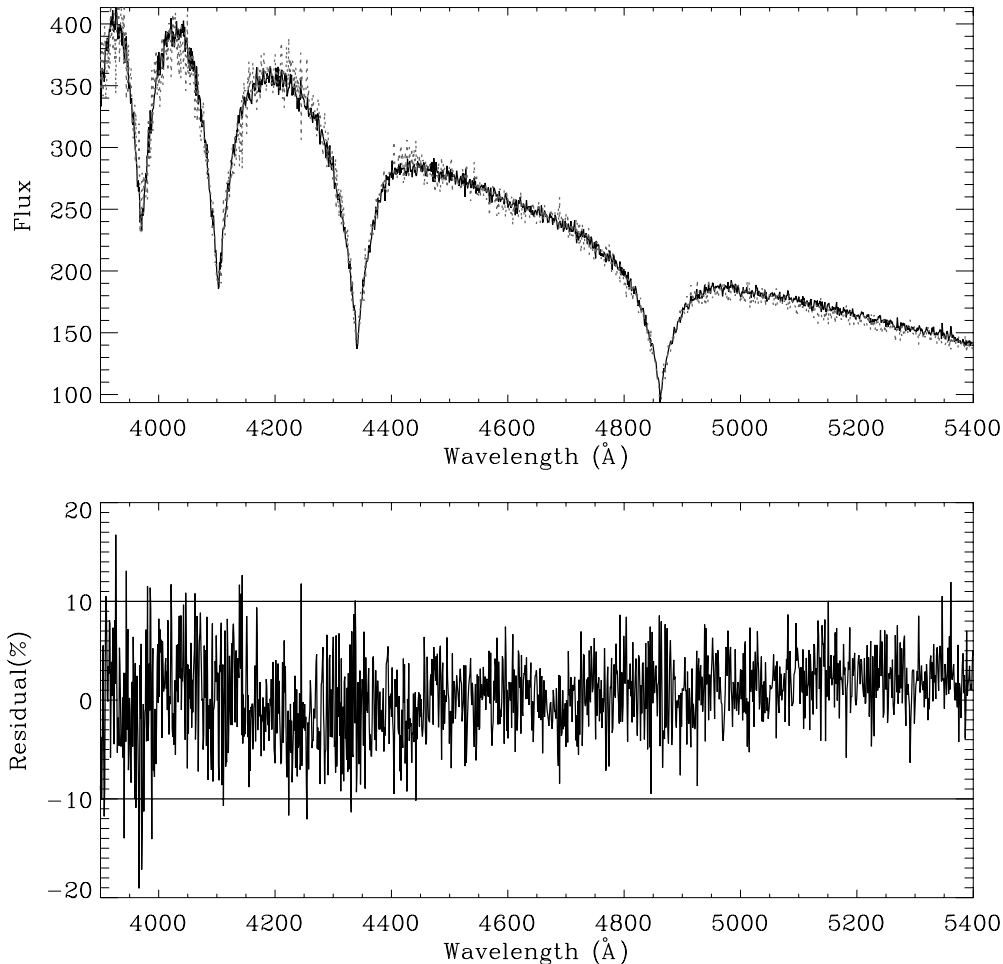
Figure 1. Comparison of typical SDSS and LAMOST pilot survey WD spectra for star J100316.35−002336.95. In the top panel, the solid line is the LAMOST spectrum while the dotted line is that from SDSS. The bottom panel presents the residual between the two spectra.

was rejected even if selected by the pipeline. After these filters, 70 DA WDs were left. Table 1 presents the physical data for these WDs. Column 1 is an ID number. Columns 2–5 list the name, R.A., and decl., respectively. The estimated T_{eff}, log g, mass, and the cooling time are given in Columns 5–8. Columns 9–13 list the apparent magnitudes of each WD. Column 14 indicates the source of the magnitudes. The last two columns are estimates of the color excess $(B - V)$ and distance. The $E(B - V)$ is estimated from Schlegel et al. (1998).

3. PARAMETER DETERMINATION

3.1. T_{eff} and log g

For our DA WD candidates, the T_{eff} and log g were derived via simultaneous fitting of the Hβ to H8 Balmer line profiles using the procedure outlined by Bergeron et al. (1992). The line profiles in both observed spectra and model spectra were first normalized using two points at the continuum level on either sides of each absorption line. Thus, the fit should not be affected by the flux calibration. Model atmospheres used for this fitting were derived from model grids provided by Koester (2010). Details of the input physics and methods can be found in that reference. Fitting of the line profiles was carried out using the IDL package MPFIT (Markwardt 2009), which is based on χ^2 minimization using Levenberg–Marquardt method. This

package can be downloaded from the project Web site.[3] Errors in the T_{eff} and log g were calculated by stepping the parameter in question away from their optimum values and redetermining minimum χ^2 until the difference between this and the true minimum χ^2 corresponded to 1σ for a given number of free model parameters.

Figures 2 and 3 show examples of T_{eff} and log g determinations for J150156.26+302300.13. Figure 2 is the contour plot of the χ^2 residual and the rough T_{eff} and log g implied by these error eclipses. Figure 3 shows the actual fits of the observed Balmer lines for J150156.26+302300.13. The black solid lines are the observed profiles of Balmer lines from Hβ to H8. The red dashed lines are the model spectra. The derived T_{eff}, log g, and uncertainties for all the WDs are shown in Columns 5 and 6 of Table 1. Estimated T_{eff} and log g values for 14 DAs were also available in the literature, allowing the comparisons shown in Figure 4. The solid line represents the unit slope relation. Plus (+) symbols represent the WDs with high S/N spectra, while squares represent WDs with low S/N spectra. The three spectra of lowest S/N are outliers in the log g comparison plot suggesting the importance of S/N in determining this parameter. For most of other WDs, the mean differences between our and the literature T_{eff} values are less than 1000 K and the log g difference is less than 0.2 dex. Within this scatter, our results are consistent with those in the literatures. One of our candidates,

_____
3 http://purl.com/net/mpfit

Table 1
Catalog of DA White Dwarfs

No.	LAMOST Obj	R.A. (deg)	Decl. (deg)	$T_{\rm eff}$ (K)	log g	Mass ($M_\odot$)	Age (Myr)	u	g	r	i	z	V	Source[a]	$E(B-V)$	dis (pc)
0	J220522.86+021837.56	331.345250	2.310432	15377 ± 493	8.02 ± 0.10	0.63 ± 0.06	190 ± 43	17.35	17.00	17.25	17.45	17.71		1	0.05	135
1	J025737.25+264047.89	44.405201	26.679970	19008 ± 669	7.87 ± 0.12	0.55 ± 0.06	66 ± 21		16.91	17.00	17.16			2	0.16	139
2	J030214.72+285707.41	45.561340	28.952057	21894 ± 1406	8.01 ± 0.23	0.64 ± 0.13	46 ± 37		17.21	17.60	17.80			2	0.18	173
3	J040449.34+280023.65	61.205600	28.006570	29302 ± 2525	8.25 ± 0.55	0.79 ± 0.33	20 ± 32		15.96	15.84	16.00			2	0.21	87
4	J004036.79+413138.79	10.153296	41.527443	13000 ± 651	7.75 ± 0.08	0.48 ± 0.04	216 ± 47		15.90	16.21	16.40			2	0.07	83
5	J003956.55+422929.55	9.985629	42.491542	18053 ± 816	7.32 ± 0.15	0.34 ± 0.05	50 ± 10		16.43	16.58	16.72			2	0.06	181
6	J004128.67+402324.09	10.369458	40.390026	25996 ± 733.	7.92 ± 0.10	0.59 ± 0.05	15. ± 3.						17.14	3	0.08	68
7	J005340.53+360116.89	13.418857	36.021358	29772 ± 158	7.96 ± 0.04	0.63 ± 0.02	9 ± 0		14.10	14.58	14.91			2	0.05	72
8	J100551.51−023417.87	151.464628	-2.571630	22072 ± 477	8.22 ± 0.07	0.76 ± 0.04	78 ± 16	15.15	15.10	15.46	15.76	16.08		1	0.05	68
9	J100316.35−002336.95	150.818141	-0.393597	22249 ± 330	7.92 ± 0.05	0.59 ± 0.03	33 ± 4	15.97	15.93	16.25	16.56	16.85		1	0.05	123
10	J100941.45−004404.55	152.422705	-0.734597	16489 ± 601	7.98 ± 0.13	0.60 ± 0.08	140 ± 45	17.36	16.98	17.24	17.44	17.74		1	0.04	148
11	J054613.53+255031.70	86.556364	25.842139	22935 ± 498	7.99 ± 0.07	0.63 ± 0.04	34 ± 10		17.33	17.62	17.78			2	1.72	27
12	J090734.26+273903.32	136.892757	27.650923	18619 ± 386	8.56 ± 0.07	0.97 ± 0.04	272 ± 39	16.31	16.08	16.37	16.64	16.89		1	0.03	72
13	J004628.31+343319.90	11.617971	34.555527	14644 ± 808	7.60 ± 0.18	0.41 ± 0.08	120 ± 47	16.83	16.33	16.40	16.53	16.75		1	0.08	112
14	J052038.36+304822.65	80.159836	30.806293	15924 ± 348	8.00 ± 0.07	0.61 ± 0.04	164 ± 28		15.38	15.68	15.88			2	0.85	24
15	J031236.50+515511.74	48.152099	51.919927	23558 ± 1966	7.93 ± 0.29	0.59 ± 0.14	25 ± 13						15.44	3	0.84	103
16	J055046.51+261220.27	87.693772	26.205631	28000 ± 1916	8.34 ± 0.39	0.84 ± 0.24	37 ± 57		15.13	15.64	15.91			2	1.50	13
17	J013938.94+291859.80	24.912266	29.316611	20934 ± 515	8.13 ± 0.08	0.70 ± 0.05	77 ± 22		17.53	17.94	18.19			2	0.05	213
18	J105811.27+475752.75	164.546942	47.964653	29532 ± 490	7.84 ± 0.11	0.56 ± 0.05	9 ± 0	17.09	17.29	17.75	18.10	18.35		1	0.01	353
19	J104311.45+490224.35	160.797708	49.040097					15.47	15.84	16.40	16.76	17.18		1	0.01	
20	J053931.86+285456.66	84.882770	28.915740	23865 ± 1774	8.63 ± 0.26	1.01 ± 0.15	147 ± 97		17.39	16.64	16.17			2	1.43	15
21	J094104.43+282224.58	145.268457	28.373495	16713 ± 438	7.86 ± 0.09	0.54 ± 0.05	109 ± 24	15.70	15.42	15.70	15.94	16.25		1	0.02	82
22	J081845.28+121952.45	124.688667	12.331236	22271 ± 531	8.34 ± 0.08	0.83 ± 0.05	100 ± 22	16.32	16.18	16.57	16.88	17.19		1	0.03	107
23	J014147.59+302135.45	25.448307	30.359846	17520 ± 367	8.17 ± 0.07	0.72 ± 0.04	162 ± 27		16.96	17.39	17.54			2	0.05	138
24	J014933.76+285610.60	27.390679	28.936279	32200 ± 631	8.33 ± 0.12	0.84 ± 0.07	17 ± 10		16.88	17.47				2	0.06	140
25	J074742.05+280945.57	116.925192	28.162658	15085 ± 596	7.66 ± 0.13	0.44 ± 0.06	117 ± 31	17.83	17.43	17.69	17.88	18.13		1	0.04	209
26	J075251.35+271513.85	118.213962	27.253847	25134 ± 711	7.94 ± 0.10	0.60 ± 0.06	19 ± 9	16.72	16.73	17.15	17.46	17.79		1	0.03	206
27	J075106.48+301726.96	117.776979	30.290822	34418 ± 580	8.21 ± 0.10	0.78 ± 0.06	9 ± 1	15.65	15.92	16.39	16.72	17.05		1	0.05	156
28	J113614.04+290130.26	174.058504	29.025072	24106 ± 255	7.80 ± 0.03	0.53 ± 0.02	20 ± 1	14.64	14.68	15.13	15.44	15.75		1	0.02	87
29	J113705.17+294757.54	174.271529	29.799317	21786 ± 160	8.58 ± 0.03	0.98 ± 0.02	174 ± 11	12.29	12.31	12.69	12.99	13.31		1	0.02	15
30	J113423.35+314606.58	173.597300	31.768494	14683 ± 832	8.02 ± 0.14	0.62 ± 0.08	219 ± 73	15.53	15.17	15.44	15.68	15.95		1	0.03	58
31	J093903.33+114418.62	144.763879	11.738506	16673 ± 815	8.75 ± 0.09	1.08 ± 0.05	513 ± 116	17.37	17.01	17.21	17.41	17.67		1	0.03	82
32	J070755.01+265102.94	106.979210	26.850817	17854 ± 893	8.87 ± 0.12	1.14 ± 0.06	554 ± 202		15.53	15.86	16.01			2	0.07	39
33	J104946.47+003635.81	162.443625	0.609947	19832 ± 550	8.08 ± 0.10	0.67 ± 0.06	87 ± 23	17.25	17.27	17.67	17.97	18.30		1	0.05	191
34	J104623.28+024236.57	161.596987	2.710158	13000 ± 728	7.73 ± 0.08	0.47 ± 0.04	211 ± 52	16.43	16.03	16.26	16.48	16.72		1	0.04	92
35	J104928.89+275423.77	162.370375	27.906603	14212 ± 681	7.68 ± 0.15	0.45 ± 0.07	148 ± 44	15.74	15.32	15.51	15.75	15.98		1	0.02	75
36	J115506.22+264924.59	178.775929	26.823497	17291 ± 679	8.47 ± 0.13	0.91 ± 0.08	285 ± 88	17.03	16.69	16.97	17.23	17.50		1	0.02	97
37	J094627.81+313211.08	146.615867	31.536411	15000 ± 2362	8.34 ± 0.20	0.82 ± 0.13	342 ± 218	17.30	16.91	17.12	17.34	17.55		1	0.02	103
38	J070057.53+284310.06	105.239692	28.719461	16000 ± 735	8.15 ± 0.13	0.70 ± 0.08	207 ± 66	17.37	16.98	17.23	17.45	17.73		1	0.08	120
39	J040613.25+465133.66	61.555205	46.859349	33026 ± 436	7.50 ± 0.10	0.45 ± 0.03	6 ± 1						14.77	3	0.82	145
40	J103535.22+395502.27	158.896764	39.917298	16652 ± 550	8.05 ± 0.11	0.65 ± 0.07	155 ± 39	17.43	17.12	17.33	17.55	17.84		1	0.01	154
41	J105443.36+270658.42	163.680650	27.116228	24915 ± 131	8.38 ± 0.02	0.86 ± 0.02	74 ± 4	13.86	13.98	14.34	14.64	14.97		1	0.02	41
42	J064452.84+260947.75	101.220170	26.163263	16835 ± 598	7.78 ± 0.13	0.50 ± 0.04	90 ± 20		15.48	15.98	16.22			2	0.10	86
43	J065601.55+115745.85	104.006460	11.962736	31347 ± 603	7.42 ± 0.15	0.41 ± 0.05	8 ± 1	14.31	13.48	13.13	11.94			1	0.22	63
44	J013914.45+290057.61	24.810197	29.016003	16808 ± 478	8.06 ± 0.10	0.65 ± 0.06	153 ± 34		16.20	16.53	16.68			2	0.06	97
45	J094126.79+294503.39	145.361630	29.750942	21798 ± 267	8.15 ± 0.04	0.72 ± 0.03	68 ± 10	15.88	15.91	16.25	16.55	16.87		1	0.02	106
46	J100549.01+424804.68	151.454200	42.801300	23923 ± 812	8.11 ± 0.12	0.70 ± 0.07	38 ± 13	16.04	16.00	16.39	16.70	16.98		1	0.01	127

Table 1
(Continued)

No.	LAMOST Obj	R.A. (deg)	Decl. (deg)	$T_{\rm eff}$ (K)	log g	Mass ($M_\odot$)	Age (Myr)	u	g	r	i	z	V	Source[a]	E(B − V)	dis (pc)
47	J093047.11+160012.98	142.696300	16.003606	32492 ± 634	8.00 ± 0.13	0.66 ± 0.07	7 ± 1	16.35	16.64	17.12	17.50	17.84		1	0.04	249
48	J093451.69+171814.00	143.715358	17.303889	14645 ± 566	7.80 ± 0.12	0.50 ± 0.06	156 ± 45	17.10	16.79	17.09	17.36	17.66		1	0.03	143
49	J092518.36+180534.20	141.326500	18.092833	26274 ± 324	8.29 ± 0.06	0.81 ± 0.04	43 ± 11	16.07	16.17	16.61	16.94	17.23		1	0.05	127
50	J052147.24+283532.50	80.446823	28.592361	18917 ± 466	7.81 ± 0.09	0.52 ± 0.05	59 ± 16		17.50	17.73	17.86			2	0.62	108
51	J071223.81+260933.41	108.099190	26.159281	14278 ± 632	7.75 ± 0.14	0.48 ± 0.06	159 ± 40		16.85	17.24	17.41			2	0.08	141
52	J102521.36+455553.91	156.338987	45.931643	23547 ± 908	7.51 ± 0.13	0.41 ± 0.05	19 ± 3	18.12	18.27	18.60	18.89	19.26		1	0.02	530
53	J101806.60+455830.36	154.527482	45.975101	22475 ± 1541	8.36 ± 0.22	0.85 ± 0.14	101 ± 59	17.61	17.55	17.90	18.19	18.47		1	0.01	201
54	J033149.69+305944.92	52.957023	30.995811	19435 ± 332	8.64 ± 0.06	1.02 ± 0.03	277 ± 37		16.89	17.41	17.67			2	1.18	25
55	J033253.91+284006.91	53.224625	28.668586	19000 ± 1400	9.84 ± 0.09	1.20 ± 0.15	155 ± 0		17.06	17.41	17.58			2	0.25	27
56	J090918.99+292929.61	137.329125	29.491558	22588 ± 346	8.04 ± 0.05	0.65 ± 0.03	43 ± 8	15.74	15.68	16.04	16.34	16.59		1	0.02	107
57	J102155.50+405014.85	155.481261	40.837458	23364 ± 999	7.96 ± 0.15	0.61 ± 0.09	28 ± 18	16.19	16.25	16.61	16.91	17.23		1	0.01	153
58	J121336.54+314808.77	183.402250	31.802436	13308 ± 405	8.26 ± 0.08	0.77 ± 0.05	418 ± 67	16.21	15.79	16.00	16.21	16.49		1	0.01	60
59	J134922.51−003503.15	207.343783	-0.584208	16401 ± 1151	8.52 ± 0.19	0.94 ± 0.12	363 ± 153	17.24	16.91	17.25	17.46	17.73		1	0.03	99
60	J144433.83−005958.83	221.140967	-0.999675	12165 ± 856	8.01 ± 0.21	0.61 ± 0.13	367 ± 154	16.58	16.20	16.38	16.58	16.85		1	0.04	77
61	J112518.85+541936.65	171.328550	54.326847	15272 ± 209	7.85 ± 0.04	0.53 ± 0.02	147 ± 14	15.62	15.28	15.57	15.83	16.08		1	0.01	73
62	J113203.47+065509.52	173.014441	6.919311	12455 ± 1141	7.93 ± 0.45	0.57 ± 0.25	310 ± 201	15.21	14.89	15.13	15.35	15.64		1	0.04	46
63	J084107.69+163221.71	130.282053	16.539363	16626 ± 580	8.30 ± 0.11	0.80 ± 0.07	237 ± 64	17.52	17.22	17.45	17.67	17.97		1	0.02	134
64	J150156.26+302300.13	225.484400	30.383369	27051 ± 339	7.84 ± 0.05	0.56 ± 0.03	12 ± 1	14.13	14.24	14.71	14.96	15.32		1	0.02	77
65	J063406.26+025401.30	98.526074	2.900361	31607 ± 1274	7.82 ± 0.31	0.56 ± 0.14	7 ± 1							4	1.60	
66	J064438.16+030704.39	101.159020	3.117885	12067 ± 2288	8.37 ± 0.65	0.84 ± 0.42	650 ± 791		14.10	13.66	13.51			2	1.02	5
67	J063517.47+054917.94	98.822796	5.821650	22885. ± 3739	7.48 ± 0.54	0.40 ± 0.14	21 ± 13		14.19	13.96	13.84			2	0.41	38
68	J152130.83−003055.70	230.378443	-0.515472	13000 ± 1056	7.63 ± 0.10	0.42 ± 0.05	186. ± 71.	15.52	15.24	15.53	15.78	16.09		1	0.07	67
69	J191927.67+395839.30	289.865292	39.977583	20376 ± 345	7.93 ± 0.06	0.59 ± 0.03	54 ± 8							4	0.14	

Note. [a] 1: SDSS; 2: Xuyi Schmidt Telescope Photometric Survey of the Galactic Anti-center; 3: UCAC; 4: *Kepler*.
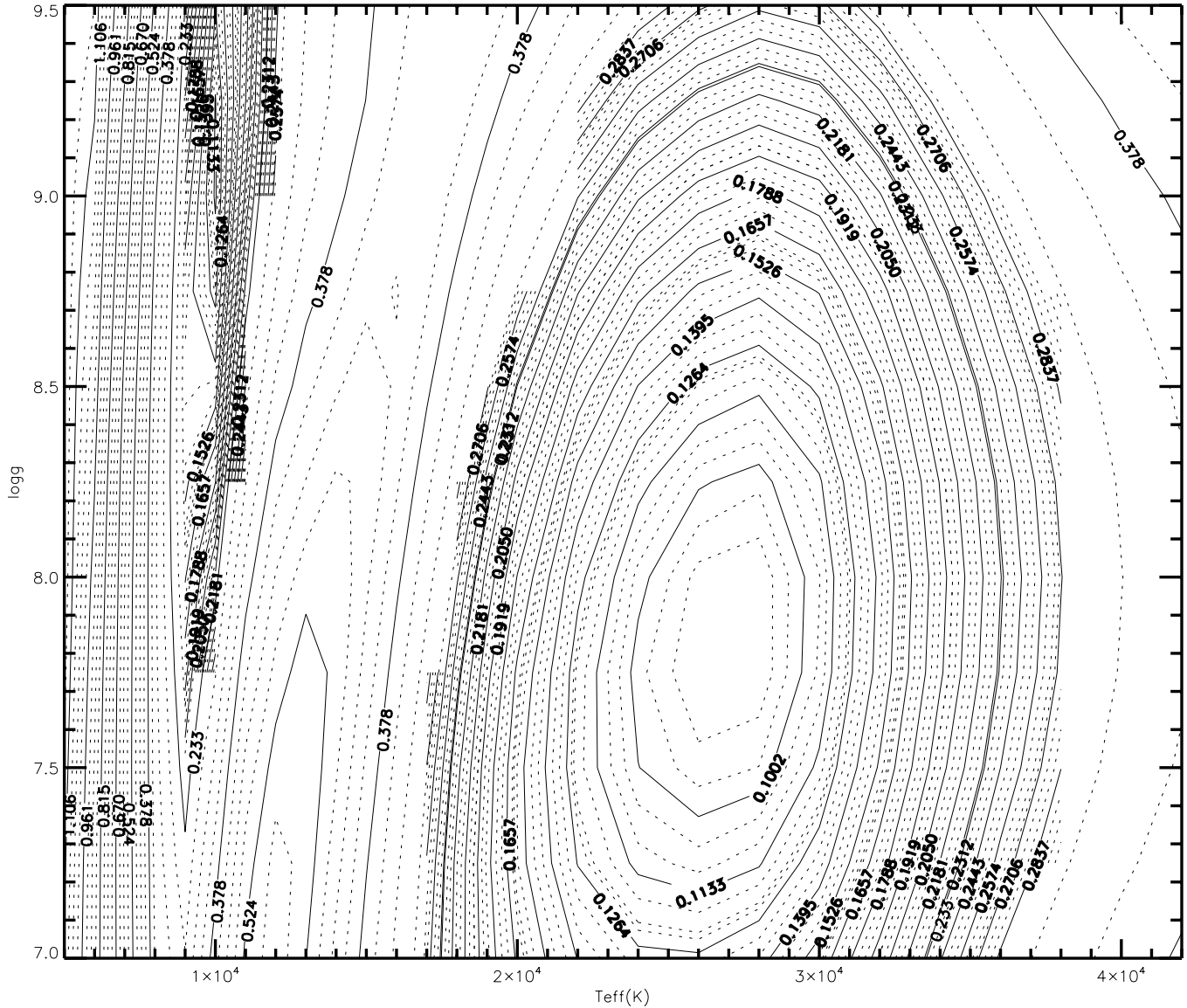
Figure 2. χ^2 contour plot of $T_{\rm eff}$ and $\log g$ determination.

J104311.45+490224.35 has also been identified as DA WD by
McCook & Sion (1999). However, we were unable to determine
its $T_{\rm eff}$ and $\log g$ because Hβ was not included in the spectrum
we obtained.

3.2. Mass and Cooling Time

From the $T_{\rm eff}$ and $\log g$ of each WD, its mass ($M_{\rm WD}$) and
cooling time ($t_{\rm cool}$) were estimated from Bergeron's cooling
sequences.[4] For the model atmospheres above $T_{\rm eff} = 30,000$ K
we used the carbon-core cooling models of Wood (1995), with
thick hydrogen layers of $q_{\rm H} = M_{\rm H}/M_* = 10^{-4}$. For $T_{\rm eff}$ below
30,000 K, we used cooling models similar to those described in
Fontaine et al. (2001) but with carbon–oxygen cores and $q_{\rm H} =$
10^{-4} (see Bergeron et al. 2001).

Figure 5 is the mass distribution of our sample resulting from
the above procedure. Masses are found to range from 0.4 $M_\odot$
to 1.2 $M_\odot$. The curve is a Gaussian fit with a peak at about
0.61 $M_\odot$, which is consistent with the mean mass 0.613 $M_\odot$

from Tremblay et al. (2011) derived from SDSS DA WDs'
sample.

3.3. Distance

The determination of distances for WDs is very difficult
because of their low luminosity. Currently only about 300 WDs
have trigonometric parallaxes. In the absence of parallaxes,
color–magnitude relations and empirical photometric methods
are often used. Holberg et al. (2008) provided improved distance
estimates for DA WDs using multi-band synthetic photometry
tied to spectroscopic temperatures and gravities. This method
was called synthetic spectral distances (SSD). The unique
aspect of SSD is the systematic use of calibrated multi-channel
synthetic absolute magnitudes, interpolated within the grid by
the $T_{\rm eff}$ and $\log g$

$$m_i = \sum_{i=(u,g,r,i,z,V)} M_i(\log g, T_{\rm eff}) + a_i A_g + 5\log d - 5. \quad (1)$$

In this paper, the distances of WDs in our sample were
estimated using Equation (1). Here, m_i are the photometric

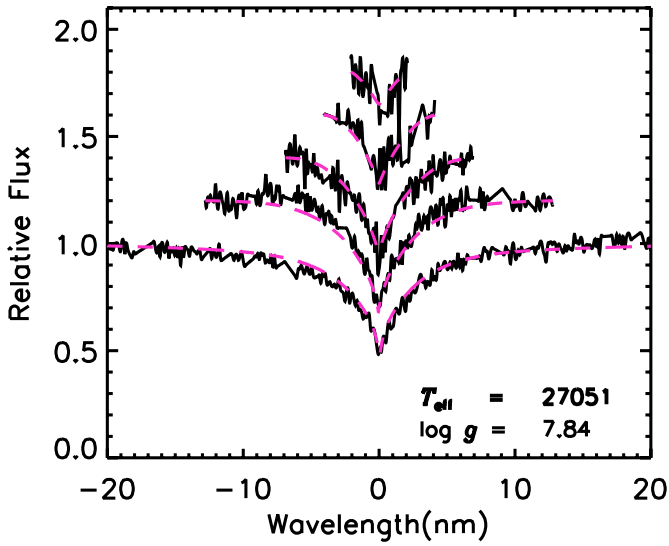[4] The cooling sequences can be downloaded from the Web site:
http://www.astro.umontreal.ca/~bergeron/CoolingModels/.

Figure 3. Fits of the observed Balmer lines for J150156.26+302300.13. Lines range from Hβ (bottom) to H8 (top). The solid black line is the observed spectra, while the dashed line is the model spectra.
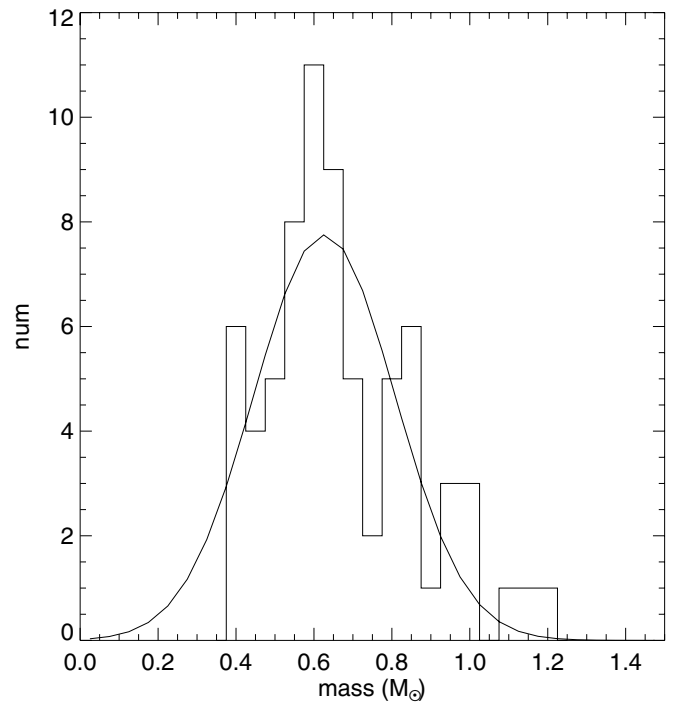
(A color version of this figure is available in the online journal.)

Figure 5. Mass distribution of our sample of candidate WDs. The curve is a Gaussian fit with a peak at about 0.61 $M_\odot$.
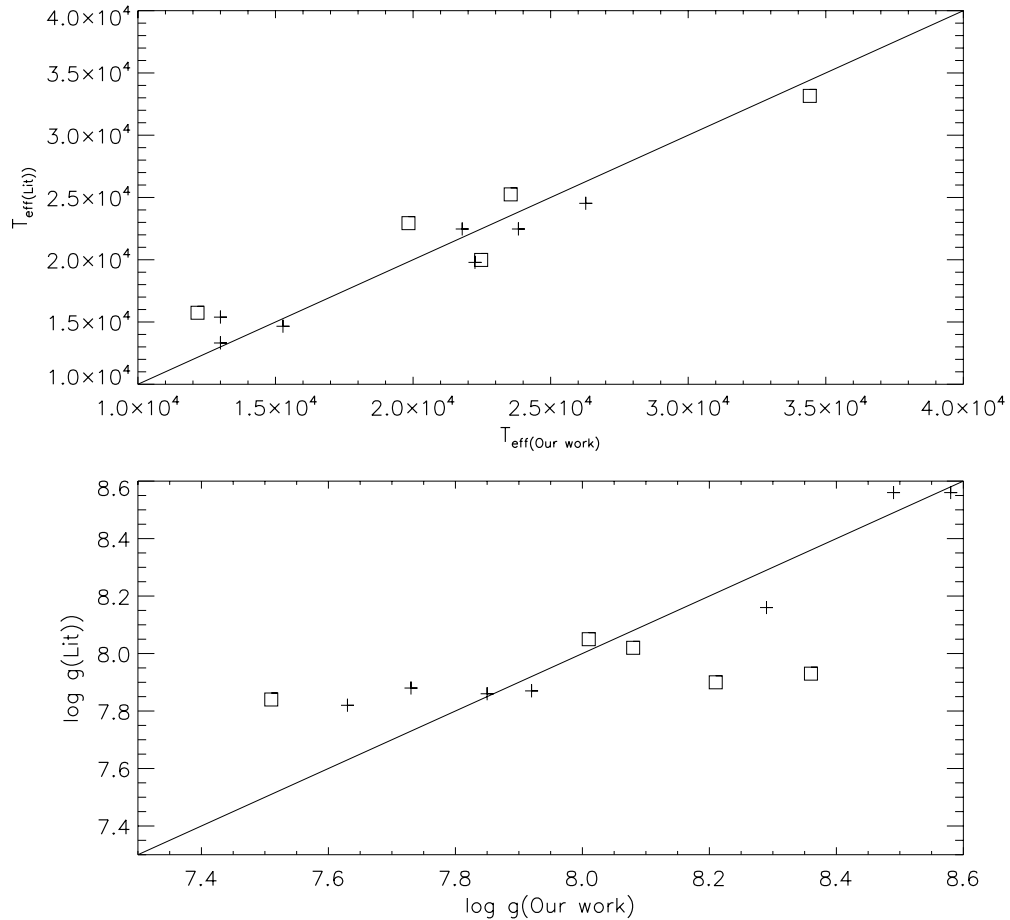
magnitudes of the WDs. Most of ours has u, g, r, i, z magnitudes. Almost all have at least g, r, and i magnitudes. A few WDs still only have V magnitude. M_i is the model absolute magnitudes calculated by interpolations in the atmospheric models provided

Figure 4. Comparison of estimated $T_{\rm eff}$ and log g values determined in this study to those from the literature. Pluses (+) represent WDs with high S/N (>20), while squares represent WDs with low S/N (<20) spectra. The solid line is the unit slope relation.

6
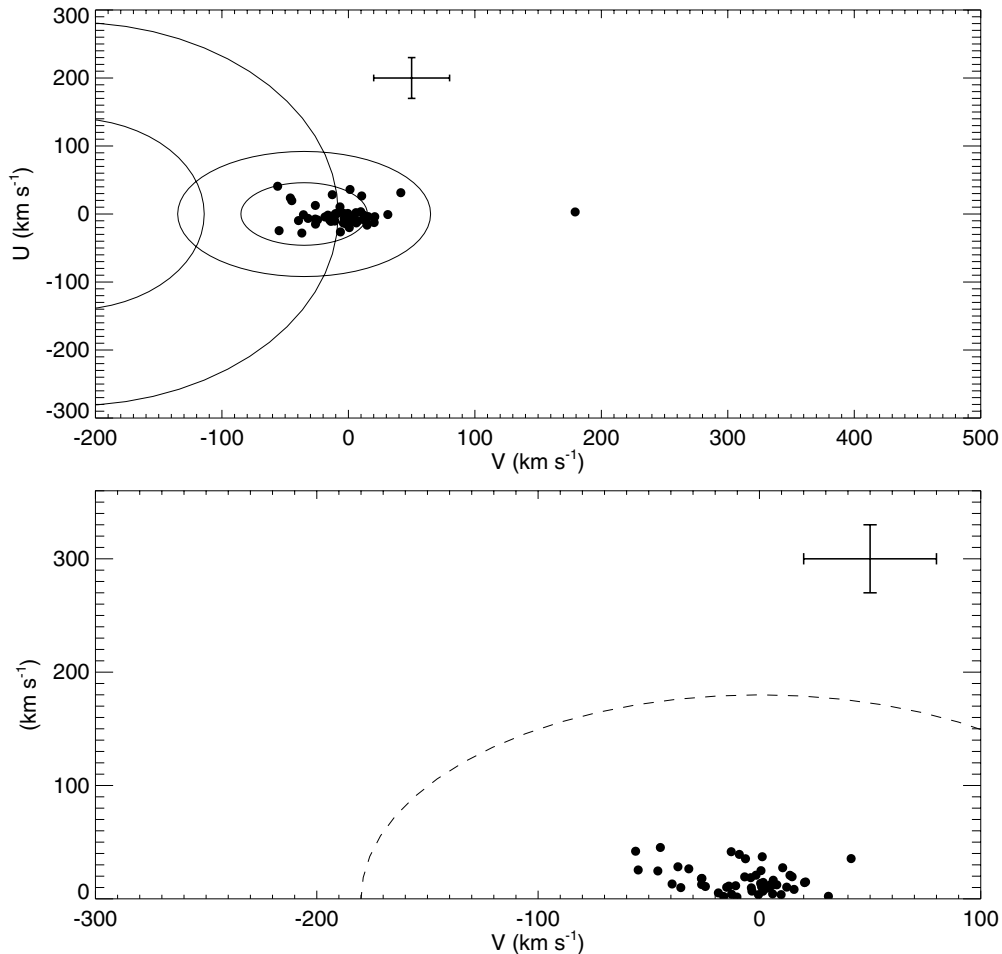
Figure 6. Top: UV–velocity distribution of our WD candidates. Ellipsoids indicate 1σ (inner) and 2σ (outer) contours for Galactic thick disk and halo populations, respectively. Bottom: Toomre diagram of our WDs. The dashed line is $V_{total} = 180$ km s^{-1}.

by Bergeron. $A_g a_i$ is the reddening and d is the distance in parsecs. In general for each magnitude a corresponding distance can be calculated. The final distance is estimated by using weighted average. The weights adopted are the errors in the magnitude. Here, we only calculated the distances for WDs having u, g, r, i, z, or V magnitude data. Distances for two WDs in Table 1 could not be estimated.

4. KINEMATICS

Oppenheimer et al. (2001) suggested that halo WDs could provide a significant contribution to the Galactic dark matters' component, which prompted much interest in WD kinematics. In a related study, Silvestri et al. (2002) observed 116 common proper-motion binaries consisting of a WD plus M dwarf component. They determined full space motions of their WDs from the companion M dwarfs. Most of their WDs were found to be members of the disk; only one potential halo WD was identified. Even the much larger samples of WDs such as the Pauli et al. (2003, 2006) SN Ia Progenitor Survey have found relatively few genuine halo and thick disk candidates. In their magnitude-limited sample of 398 WDs, they examined both the *UVW* space motions and the Galactic orbits of their stars. They found only 2% of their sample kinematically belonged to the halo and 7% to the thick disk. Sion et al. (2009) presented the kinematical properties of the WDs within 20 pc of the Sun. In their nearby sample, they found no convincing

evidence of halo members among 129 WDs, nor was there convincing evidence of genuine thick disk subcomponent members within 20 pc. The entire 20 pc sample likely belongs to the thin disk.

The proper motions of our sample were derived by the cross-correlating with PPMXL catalog (Roeser et al. 2010). Silvestri et al. (2002), Pauli et al. (2003, 2006), and Sion et al. (2009) found relatively little kinematical difference among the samples whether they used radial velocity (RV) to compute full space motions or used the simple zero RV for simple WDs. We have assumed zero RVs in the analysis of our sample. U is measured positive in the direction of the Galactic anti-center, V is measured positive in the direction of the Galactic rotation, and W is measured positive in the direction of the north Galactic pole. The U, V, and W velocities were corrected for the peculiar solar motion $(U, V, W) = (-9, +12, +7)$ km s^{-1} (Wielen 1982). The space motions of 59 WDs with sufficient kinematical information (photometric or trigonometric parallax, proper motion) in our sample were calculated.

The top panel of Figure 6 shows contours, centered at $(U, V) = (0, -220)$ km s^{-1}, that represent 1σ and 2σ velocity ellipsoids for stars in the Galactic stellar halo as defined by Chiba & Beers (2000). Only one of our candidate WDs lies outside the 2σ velocity contour centered on $(U, V) = (0, -35)$ km s^{-1} defined for disk stars (Chiba & Beers 2000). The bottom of Figure 6 shows a Toomre diagram for our stars. Venn et al. (2004) suggested that stars with $V_{total} > 180$ km s^{-1} are possible halo
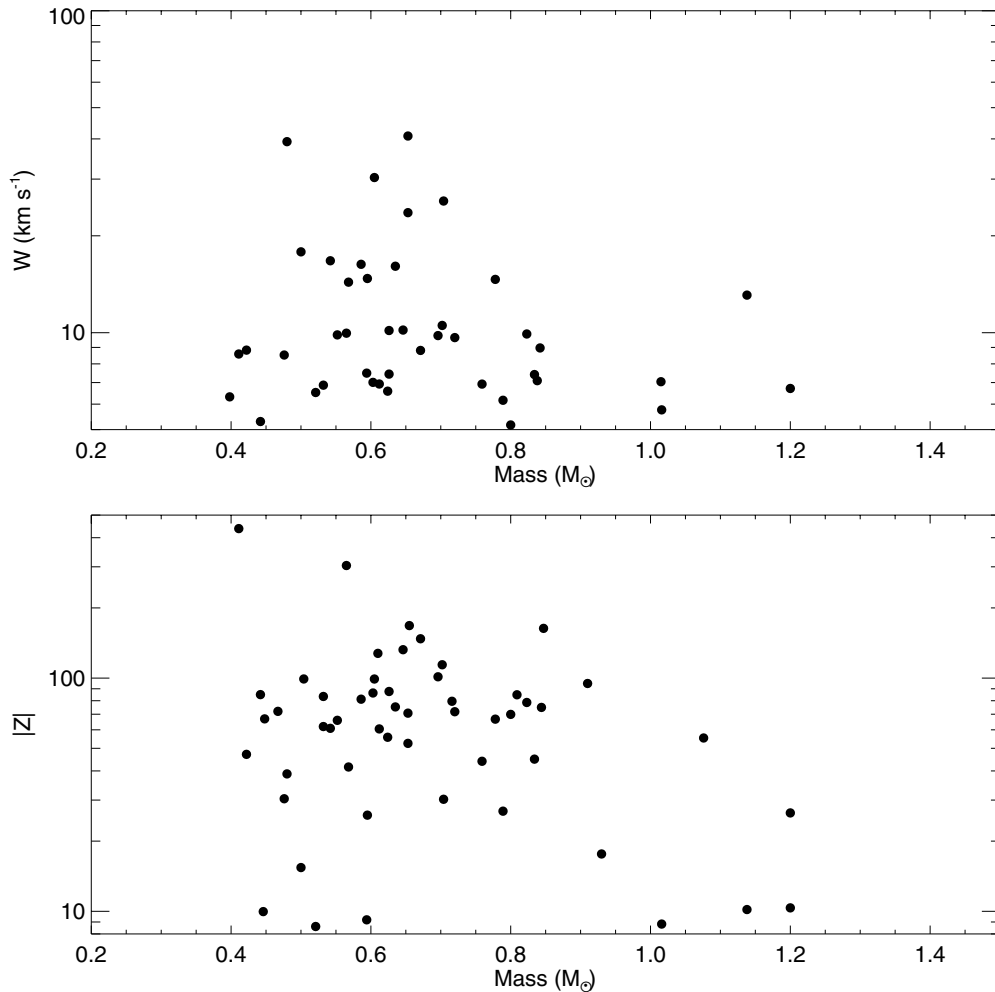
Figure 7. Top: *W* vs. mass. Bottom: |*Z*| vs. mass. Lower mass WDs clearly tend to have larger dispersion in both *W* velocity and vertical distance of the Galactic plane |*Z*|.

members. None of our stars meet this criterion. We conclude that our sample consists entirely of disk stars.

Wegg & Phinney (2012) concluded that kinematical dispersion decreases with increasing WD mass among young WDs whose cooling time is smaller than 3×10^8 yr. Progenitors of high-mass WDs have shorter lifetimes, hence they should be closer to the Galactic plane and have small kinematical dispersion in accord with the disk "heating" theory. Since most WDs in our sample are relatively young, we investigated the relation between mass and *W*, as well as mass and the vertical distance of the Galactic plane |*Z*| (see Figure 7). In the top panel of Figure 7, WDs with mass larger than 0.8 $M_\odot$ are seen to have smaller *W*. Also, the vertical distances from the Galactic plane of WDs with larger mass are relative small. Although there is no strict relation such as seen in Wegg & Phinney (2012), our sample supports the general expectation that high-mass WDs tend to have lower *W* and |*Z*|.

5. CONCLUSIONS

From the LAMOST pilot survey data, 70 DA WDs were detected with S/N > 10. T_{eff}, log *g*, cooling time, mass, and distance of these WDs were determined from their spectra. The T_{eff} of most WDs range from 12,000 K to 35,000 K and the cooling times of all the WDs are younger than 300 Myr. All these WDs were found to be members of Galactic disk. WDs

with higher mass tend to have smaller vertical distance from the Galactic disk, which partly supports the conclusions of Wegg & Phinney (2012).

The DA WD catalog of the LAMOST pilot survey provides a first glimpse of how useful the survey will be to search for nearby WDs. The upcoming formal LAMOST survey will enlarge the sample of WDs rapidly, perhaps providing the largest sample of WDs available. This large sample will open the door to much more detailed investigation of the physical and kinematic properties of WDs in the solar neighborhood as well as the local structure and evolution of the Galaxy.

the National Astronomical Observatories, Chinese Academy of Sciences.

REFERENCES

Bergeron, P., Leggett, S. K., & Ruiz, M. T. 2001, ApJS, 133, 413
Bergeron, P., Saffer, R. A., & Liebert, J. 1992, ApJ, 394, 228
Carlin, J. L., Lépine, S., Newberg, H. J., et al. 2012, RAA, 12, 755
Chen, L., Hou, J., Yu, J., et al. 2012, RAA, 12, 805
Chiba, M., & Beers, T. C. 2000, AJ, 119, 2843
Cui, X., Zhao, Y., Chu, Y., et al. 2012, RAA, 12, 1197
Eisenstein, D. J., Liebert, J., Harris, H. C., et al. 2006, ApJS, 167, 40
Fontaine, G., Brassard, P., & Bergeron, P. 2001, PASP, 113, 409
Fontaine, G., & Wesemael, F. 2000, in Encyclopedia of Astronomy and Astrophysics 1894–1901, ed. P. Murdin (Bristol: IOP), 1894
Harris, H. C., Liebert, J., Kleinman, S. J., et al. 2003, AJ, 126, 1023
Holberg, J. B., Bergeron, P., & Gianninas, A. 2008, AJ, 135, 1239
Kleinman, S. J., Harris, H. C., Eisenstein, D. J., et al. 2004, ApJ, 607, 426
Kleinman, S. J., Kepler, S. O., Koester, D., et al. 2013, ApJS, 204, 5
Koester, D. 2010, MmSAI, arXiv:0812.0482
Krzesinski, J., Kleinman, S. J., Nitta, A., et al. 2009, A&A, 508, 339
Luo, A. L., Zhang, Y. X., & Zhao, Y. H. 2004, SPIE, 5496, 756
Luo, A. L., Zhang, H. T., Zhao, Y. H., et al. 2012, RAA, 12, 1243
Markwardt, C. B. 2009, in ASP Conf. Ser. 411, Non-linear Least Squares Fitting in IDL with MPFIT, Proc. Astronomical Data Analysis Software and Systems XVIII, Quebec, Canada, ed. D. Bohlender, P. Dowler, & D. Durand (San Francisco, CA: ASP), 251
Mccook, E. P., & Sion, E. M. 1999, ApJS, 121, 1
Oppenheimer, B. R., Hambly, N. C., Digby, A. P., Hodgkin, S. T., & Saumon, D. 2001, Sci, 292, 698
Pauli, E.-M., Napiwotzki, R., Altmann, M., Heber, U., & Odenkirchen, M. 2003, A&A, 400, 877
Pauli, E.-M., Napiwotzki, R., Heber, U., Altmann, M., & Odenkirchen, M. 2006, A&A, 447, 173
Roeser, S., Demleitner, M., & Schilbach, E. 2010, AJ, 139, 2440
Salaris, M., Garca-Berro, E., Hernanz, M., Isern, J., & Saumon, D. 2000, ApJ, 544, 1036
Schlegel, D. J., Finkbeiner, D. P., & Davis, M. 1998, ApJ, 500, 525
Silvestri, N. M., Oswalt, T. D., & Hawley, S. L. 2002, AJ, 124, 1118
Sion, E. M., Holberg, J. B., Oswalt, T. D., McCook, G. P., & Wasatonic, R. 2009, AJ, 138, 1681
Tremblay, P.-E., & Bergeron, P. 2009, ApJ, 696, 1755
Tremblay, P. E., Bergeron, P., & Gianninas, A. 2011, ApJ, 730, 128
Venn, K. A., Irwin, M., Shetrone, M. D., et al. 2004, AJ, 128, 1177
Wang, S. G., Su, D. Q., Chu, Y. Q., Cui, X., & Wang, Y. N. 1996, ApOpt, 35, 5155
Wegg, C., & Phinney, E. S. 2012, MNRAS, 426, 427
Wielen, R. 1982, Landolt-Börnstein Tables, Astrophysics, Vol. 2C, Sec. 8.4 (Berlin: Springer), 202
Wood, M. 1995, in White Dwarfs, ed. D. Koester & K. Warner (Berlin: Springer), 41
Yang, F., Carlin, J. L., Newberg, H. J., et al. 2012, RAA, 12, 781
York, D. G., Adelman, J., Anderson, J. E., Jr., et al. 2000, AJ, 120, 1579
Zhang, Y., Carlin, J., Liu, C., et al. 2012, RAA, 12, 792